



Land-snail eggs from Chinese L9 loess strata and seasonal cooling events during Marine Isotope Stages 24–22

Fengjiang Li ^{a,*}, Naiqin Wu ^a, Denis-Didier Rousseau ^{b,c,d}, Linpei Huang ^e, Bin Wu ^f, Qingzhen Hao ^a, Yajie Dong ^a, Xiaoyun Chen ^g

^a State Key Laboratory of Lithospheric and Environmental Coevolution, Institute of Geology and Geophysics, Chinese Academy of Sciences, Beijing, 100029, China

^b Geosciences Montpellier, University of Montpellier, 34095, Montpellier, France

^c Institute of Physics-CSE, Division of Geochronology and Environmental Isotopes, Silesian University of Technology, Gliwice, Poland

^d Lamont-Doherty Earth Observatory, Columbia University, Palisades, NY, 10964, USA

^e Yunnan Key Laboratory of Plateau Geographical Processes and Environmental Change, Faculty of Geography, Yunnan Normal University, Kunming, 650500, China

^f Technical Centre for Soil, Agriculture and Rural Ecology and Environment, Ministry of Ecology and Environment, Beijing, 100012, China

^g The Geological Museum of China, Beijing, 100034, China

ARTICLE INFO

Handling Editor: Dr Mira Matthews

Keywords:

Land-snail egg

Seasonal cooling event

Loess

Marine Isotope Stages 24–22

The Mid-Pleistocene transition

ABSTRACT

Knowledge of the long-term evolution of seasonal cooling events contributes to our understanding of glacial-interglacial cycles. Recently, using land-snail eggs as a proxy, we have reconstructed the evolution of seasonal cooling events during glacial-interglacial cycles of the last 490 ka, corresponding to Marine Isotope Stages (MIS) 12–1. During this time interval, seasonal cooling events are strong during most climate cooling shifts. However, it is unclear how such events evolved under climate conditions significantly different from those during the last five climatic cycles. As the ending segment of the Mid-Pleistocene Transition (MPT), MIS 24–22 (~940–870 ka) yields different climate conditions from those during the last five climatic cycles. Here we present two parallel land-snail egg records from the entire L9 loess and the upper part of the underlain S9 paleosol of the Chinese Loess Plateau (CLP), covering the time interval between 950 and 860 ka. Our results show that land-snail egg abundance documents four strong seasonal cooling events (SE-4 to SE-1). SE-4 and SE-2 occur during climate cooling transitions of MIS 25/24 and MIS 23/22, respectively; SE-3 and SE-1 occur near the glacial maxima of MIS 24 and MIS 22, respectively. This indicates that during the ending interval of the MPT, seasonal cooling events occurred during both climate cooling transitions and glacial maxima, but over the last five glacial-interglacial cycles, they mainly occurred during climate cooling transitions, as indicated by our previous results. The cooling-transition events, SE-4 and SE-2, are stronger than the glacial-maximum ones, SE-3 and SE-1. They do not seem to occur during deglacials and the warming maximum of MIS 23. These results lead us to infer that the occurrence of seasonal cooling events seems to be more closely related to ice-sheet growth at high northern latitudes. A certain amount of ice-sheet growth with low concentrations of ice-raftered debris at high northern latitudes could have strengthened seasonal cooling events over the CLP. However, during the last several glacial maxima, the Northern Hemisphere ice volumes could have been sufficiently large to diminish variability that does not favor the occurrences of seasonal cooling events in the CLP. Moreover, decreases in local spring insolation are also likely to have facilitated the occurrence of seasonal cooling events. Our study provides the first evidence to understand the evolution of seasonal cooling events during the ending segment of the MPT.

1. Introduction

Seasonality has long been viewed as a crucial factor responsible for long-term climate changes, such as glacial-interglacial cycles (e.g., Crowley et al., 1986; Haug et al., 2005) and millennial oscillations (e.g.,

Denton et al., 2005). Recently, the long-term evolution of seasonal events has been specifically investigated. Phytolith record has well indicated that in tropical East Asia seasonal drought events are absent during the Holocene, but are strong during the last glacial, which is consistent with large sea-surface temperature gradients in the tropical

* Corresponding author.

E-mail address: fengjiangli@mail.igcas.ac.cn (F. Li).

Pacific (Zhang J.P. et al., 2020). This study confirmed that investigation of the evolution of seasonal events is likely to provide learning insight about long-term climate changes. However, the time coverage of this previous study, although demonstrative, remains insufficient. Older glacial-interglacial cycles have to be investigated to apprehend properly and give a complete picture of the evolution of seasonal events under different glacial-interglacial climatic conditions. A long timeseries of seasonally sensitive proxies is fundamental for such investigations.

Land-snail eggs are a novel and reliable proxy of seasonal cooling events (Li et al., 2021, 2022), based on the principle that egg hatching is sensitive to temperature changes during the reproductive season (e.g., Barker, 2001; Sun, 2001; Brown et al., 2004; Welter-Schultes, 2012). This is also supported by recent investigations of modern land-snail eggs across the Chinese Loess Plateau (CLP) and East China. Higher egg abundance occurs in the CLP where cold spells are stronger and therefore determined lower spring temperatures which are unfavorable for egg hatching. However, in East China, egg abundance is much lower than in the CLP because the weakest cold spells there do not alter the higher spring minimum temperatures which are suitable for egg hatching (Li et al., 2021). Fossil land-snail eggs are abundant in loess deposits of the CLP over the last 1.3 Ma (Li et al., 2019), providing us with a unique proxy to investigate the evolution of seasonal cooling events during glacial-interglacial cycles.

The loess-paleosol sequences in the CLP are among the best continuous terrestrial records of Quaternary climate change (e.g., Liu et al., 1958; Wang et al., 1962; Lu and An, 1979; Liu, 1985; Kukla, 1987; Kukla and An, 1989; Ding et al., 1995, 2002; Rousseau and Wu, 1997, 1999; Guo et al., 1998; Lu et al., 1999, 2004, 2022; Wu et al., 2007, 2018; Rousseau et al., 2009; Sun et al., 2010; Wu and Wu, 2011; Hao et al., 2012; Meng et al., 2018; Zhang Y.T. et al., 2020). First, stratigraphically, alternations of loess (L) and paleosol (S) units document the glacial-interglacial cycles of the last 2.6 Ma through their correlation with the cycles of even and odd Marine Isotope Stage (MIS) (Fig. 1) (e.g., Liu, 1985; Lisiecki and Raymo, 2005). Loess and even MIS correspond to glacials, while paleosols and odd MIS represent interglacials (e.g., Liu et al., 1958; Lisiecki and Raymo, 2005). Second, spatially, loess deposits in the CLP cover ~273,000 km², and the loess sequences at most sites show a complete stratigraphy, with all loess and paleosol units being spatially correlated, especially for the last ~1.3 Ma (e.g., Liu, 1985; Kukla and An, 1989; Kukla et al., 1990; Ding et al., 2002; Hao et al., 2012).

The loess and paleosol units of the last ~1 Ma over the CLP are classically labeled, from bottom to top, S9, L9, S8, L8 ... S2, L2, S1, L1 and the Holocene paleosol S0 (Fig. 1) (Lu and An, 1979; Liu, 1985; Kukla, 1987). We have recently investigated land snail eggs preserved in the L5, S4, L4, S3, L3, S2, L2, S1, L1 and S0 units in the western CLP and reconstructed the history of seasonal cooling events over the last five glacial-interglacial cycles covering the last 490 ka (Li et al., 2022, 2023). A new phenomenon has been observed that during the last five glacial-interglacial cycles, strong seasonal cooling events mainly occur during most climate cooling shifts, such as glacial inceptions, but are absent from deglacials and interglacial maxima, indicating a potential relationship with the ice-sheet dynamics at high northern latitudes (Li et al., 2022, 2023). These studies document, for the first time, seasonal cooling events at the glacial-interglacial timescale, but it was restricted to the analysis of the last five climatic cycles. Therefore, extension of the dataset to deeper past enables the investigation of seasonal events over more glacial-interglacial cycles with different climate conditions from the last 490 ka.

MIS 24–22 (~940–870 ka) time interval is the ending segment of the Mid-Pleistocene Transition (MPT, between 1.25 and 0.7 Ma (Clark et al., 2006)), yielding climate conditions (mainly in periodicity – transition from the 41 ka to 100 ka cycles - and ice volume – expansion of Northern Hemisphere ice sheets) largely different from those during the last five climatic cycles (Lisiecki and Raymo, 2005). The L9 loess unit over the CLP is subdivided upwards as L9LL2, L9SS1 and L9LL1 which

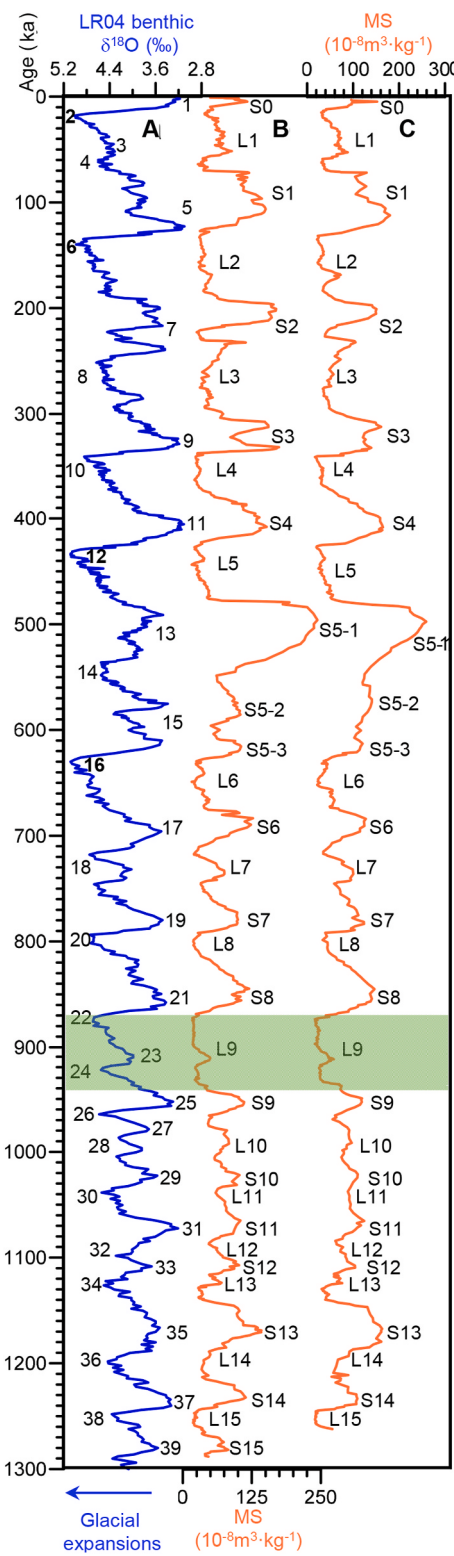


Fig. 1. Correlation between Marine Isotope Stages (MIS) and Chinese loess and paleosol units. A. Benthic $\delta^{18}\text{O}$ stack LR04 (Lisiecki and Raymo, 2005). Numbers indicate MIS. B and C. Magnetic susceptibility (MS) records from the Xifeng and Luochuan loess sequences, respectively. The major loess (L15–L1) and paleosol units (S15–S0) are indicated after Liu (1985) and Kukla and An (1989).

correspond to MIS 24, MIS 23 and MIS 22, respectively, and the underlain S9 paleosol is consistent in age with MIS 25 (Liu, 1985; Kukla, 1987; Kukla and An, 1989; Wu and Wu, 2011). The loess-paleosol sequence provides therefore an appropriate terrestrial record for studying the potential evolution of seasonal cooling events during this key transitional time interval of the MPT.

Discovery of the L9 loess unit can be traced back to the mid-1950s (Liu et al., 1958; Wang et al., 1962), but until the 1970s it was formally named L9 in the Luochuan section by Lu and An (1979). The L9 unit was identified as one of the stratigraphic markers of loess deposits in China because of its pale color, coarse texture, loose cementation and huge thickness (Liu, 1985; Wu and Wu, 2011). The coarse texture likely indicates harsher windy conditions that allow the emission, transport and deposition of coarser material (e.g., Liu, 1985; Kukla and An, 1989). Afterwards, numerous studies were specifically conducted on the L9 loess unit, about various topics including lithology, stratigraphy, sedimentology and paleoclimatology (e.g., Guo et al., 1998; Zhou and Shackleton, 1999; Lu et al., 2000; Sun and Liu, 2000; Wang X.S. et al., 2005; Jin and Liu, 2011; Wang D.J. et al., 2010; Wu and Wu, 2011).

We present here two parallel time series of land-snail eggs from the L9 loess sub-units of the classic Xifeng and Luochuan loess sequences in the central CLP. Our objective is to detect potential seasonal cooling events during MIS 24–22. We first describe both studied sequences and field work protocol applied. The following section presents the results of the laboratory analyses with the description of four particular events that are discussed in the Discussion section. There, we discuss both similarities and differences in seasonal cooling events during MIS 24–22 and the last several climatic cycles and propose a possible climatic scenario.

2. Materials and methods

The CLP is situated at the latitudes of $\sim 34^{\circ}$ – 41° N and longitudes of $\sim 102^{\circ}$ – 114° E (Liu, 1964). The renowned Xifeng ($35^{\circ}46'N$, $107^{\circ}41'E$, 1350 m above sea level) and Luochuan ($35^{\circ}45'N$, $109^{\circ}25'E$, 950 m above sea level) loess-paleosol sequences are located in the central part of the CLP, with Xifeng being about 160 km west of Luochuan (Fig. 2). The current climate in the CLP is dominated by the East Asian monsoon circulations (Qian, 1991; Ding et al., 1995; Hao et al., 2012). In winter, the East Asian winter monsoon prevails and results in very unfavorable cold, dry climatic conditions for the reproduction and growth of most plants and animals. In spring, most plants and animals initiate their reproductions. However, seasonal cooling events, exemplified by cold spells, are also frequent in spring and they can cause rapid decreases in

temperature of over 8 – 10 °C (e.g., Qian, 1991; Han et al., 2013). Such low temperatures strongly affect the hatching of land-snail eggs (Li et al., 2021). Generally, cold spells in the northwestern CLP are stronger than in the southeastern CLP and therefore Xifeng, rather than Luochuan, tends to be more exposed to cold spells (e.g., Qian, 1991). In summer, the East Asian summer monsoon predominates, causing high precipitations and temperatures favorable for the biosphere, including land snails. The current mean annual temperature (MAT) and precipitation (MAP) are 8.3 °C and 560 mm at Xifeng, and 9 – 9.2 °C and 620 mm at Luochuan (Wu et al., 2007; Zhang Y.T. et al., 2020).

The Xifeng and Luochuan loess-paleosol sequences are globally representative loess sequences. They span the entire Quaternary, i.e., the last 2.6 Ma, with a total thickness (depth) of ~ 176 m at Xifeng and ~ 137 m at Luochuan (Liu, 1985; Kukla and An, 1989). The L9 loess unit is observed at depths from 83.8 m to 72.9 m at Xifeng and from 62.2 m to 54.3 m at Luochuan, i.e., with a thickness of 10.9 m and 7.9 m, respectively. We performed our field and laboratory work through the protocol extensively used in the studies of fossil land snails (e.g., Rousseau and Wu, 1997, 1999; Wu et al., 2002, 2007; Moine et al., 2008; Rousseau et al., 2009; Sümegei et al., 2011; Wu and Wu, 2011; Li et al., 2022, 2023; Dong et al., 2020, 2021, 2022). Continuous columns have been excavated in both sections. Each column composed of steps is ~ 1 – 1.5 m wide and ~ 1.5 – 2.5 m high. We removed about 0.5 – 1 m thickness of weathered sediments from the surface of the stratigraphy to prevent contamination from modern materials, get vertical profiles, and facilitate stratigraphy identification and sampling. We used stratigraphic markers or horizontal lines to connect the successive prepared steps of different columns, obtaining two continuous loess sequences for sampling. We took a total of 212 sediment samples (121 from Xifeng and 91 from Luochuan) at a 10-cm interval from the upper S9 to the lower S8 (Fig. 3). Each sediment sample corresponded to ~ 15 L, weighing about 15 kg (Fig. 3B). All the samples, with a total weight of over 3 tons, were carried upwards to the ground from the ~ 84 -m and 62 -m deep gullies of the two sections (Fig. 3C and D). To reduce sample weight and facilitate the collection of fossil materials, all samples were preliminarily washed and sieved in the field using a mesh of 0.5 -mm diameter (Fig. 3E–H). All the “reduced” samples (Fig. 3I) were transported to the laboratory for a more detailed sieving and precise preparation. In the laboratory, using a stereoscope Leica S4E, we collected, counted and identified all the complete snail shells and the identifiable shell fragments to estimate the numbers of individuals for each species following the method developed by Puisségur (1976). Eggs were collected and counted in parallel from the same sediment sample.

Low-frequency magnetic susceptibility (MS) is extensively used to characterize the alternations of glacial and interglacial/interstadial, with the paleosol units in the CLP showing much higher values than the loess unit (Liu, 1985; Kukla and An, 1989). A total of 212 sediment samples were taken for MS measurements, in parallel with the snail-egg samples. Each sample weighed about 20 g. All the samples were air dried in the laboratory before MS measurement. Low-frequency MS was measured using a Bartington MS2 meter.

The alternations of Chinese loess and paleosol units were initially dated using magnetostratigraphy showing that the loess-paleosol cycles correspond well to glacial-interglacial alternations (Heller and Liu, 1982; Liu, 1985; Kukla, 1987; Kukla et al., 1990). Later, more precise age controls of Chinese loess sequences were obtained using the dates of the MIS boundaries, based on the extensively accepted correlation scheme between Chinese loess and marine record (Ding et al., 2002). Hao et al. (2012) established the chronology of the Xifeng and Luochuan sections by combining the grain-size model developed by Porter and An (1995) and the interpolation between the MIS boundaries from Lisiecki and Raymo (2005). Because Hao et al. (2012) and we study the same two sections, we transferred their age model to our depths, via the correlation of MS records that were independently measured using the same equipment. Doing so, the time interval that we are investigating ranged from 948 to 860 ka.

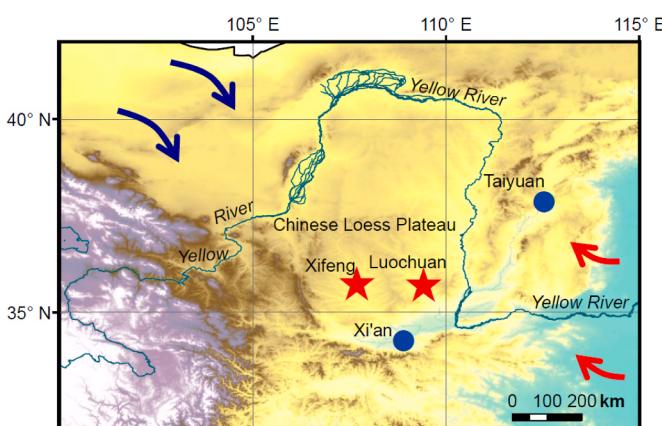


Fig. 2. Locations of the Chinese Loess Plateau and the studied sections. The red stars indicate locations of the studied Xifeng and Luochuan sections. The blue solid circles denote locations of major cities. The blue arrows indicate the direction of the East Asian winter monsoon, and the red arrows the East Asian summer monsoon.



Fig. 3. Field operations: sampling, washing and sieving of sediment samples for the collection of land-snail assemblages and their eggs. A. Sampling of loess sediment per 10-cm thickness. B. Examples of sediment samples. Each sample which is put into a bag weighs ~15 kg. C and D. Samples being transported upward from the gullies deeper than 80 m to the ground surface. E. The sediment sample is mixed with water prior to being sieved to reduce the size of the sample. F–H. Sieving samples of land-snail egg assemblages. I. Sieved sample ready to be collected and transported to the laboratory for final more precise sieving and collection of snails and eggs. The 4-cm-long green leaf in the lower left can be used as a reference scale.

3. Results

Eggs are relatively abundant, nearly all of them are well preserved, and the largest dimension of the eggs is 0.6–0.8 mm (Fig. 4). In the Xifeng section, a total of 5850 eggs were collected from 121 samples. The maximum count is 420 per 15-kg sediment at 76.1 m depth in the L9LL1 sub-unit (Fig. 5). The eggs are not evenly distributed in the L9 loess unit, but they rather concentrate on the two transitional intervals

from S9 to L9LL2, at depth of 83.5–83.1 m, and from L9SS1 to L9LL1, at depth of 79.8–78.2 m (Fig. 5; Table 1). They also occur in the mid-upper parts of both L9LL2 at depth of 82.6–81.4 m and L9LL1 at depth of 76.4–75.4 m, but the latter is a very short peak. Egg abundances during the transitions from S9 to L9LL2 and from L9SS1 to L9LL1 are stronger than those during the mid-upper parts of L9LL2 and L9LL1. They tend not to occur during warming intervals indicated by increased MS values from L9LL2 to L9SS1 and from L9LL1 to S8 (corresponding to deglacials) and by the MS peak in the L9SS1 layer (corresponding to warming maximum). Moreover, another characteristic is that the two egg-abundance peaks above the L9SS1 unit are higher (the maxima are 420 and 314 at Xifeng, respectively) than those under the L9SS1 unit (the maxima at Xifeng are 178 and 253, respectively) (Table 1).

In the Luochuan section, a total of 761 eggs were observed from 91 samples. The maximum number is 112 per 15-kg sediment at 56.3 m depth, and it also occurred in the L9LL1 sub-unit (Fig. 5). As shown in Fig. 5, land-snail egg abundance in the Luochuan sequence has a similar distribution pattern with those in the Xifeng sequence, but two differences are observed. First, the abundance of eggs is significantly lower in Luochuan than in Xifeng. Second, during the middle-upper part of L9LL2, there is no clear peak in the Luochuan section which corresponds to the lowest peak in the Xifeng section. These two differences are consistent with meteorological observation that seasonal cooling events are stronger in Xifeng than in Luochuan (Qian, 1991).

Based on our previous interpretation inferred from peaks in egg abundance (Li et al., 2021, 2022, 2023), our new observations allow us to distinguish four seasonal cooling event intervals. We named these seasonal event intervals (SE) as SE-1, SE-2, SE-3 and SE-4 from top to bottom (we use ascending order to name the seasonal events for consistency with the numbering rule of loess-paleosol and MIS). The

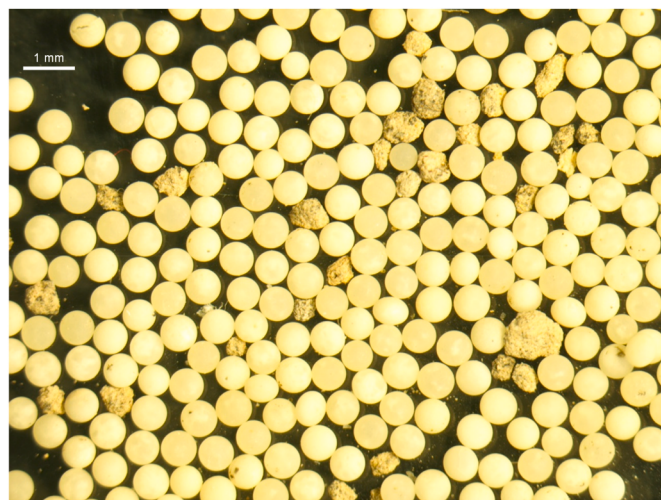


Fig. 4. Well preserved fossil land-snail eggs from the L9 loess unit of the Xifeng loess-paleosol sequence, with a few angular remaining loess material.

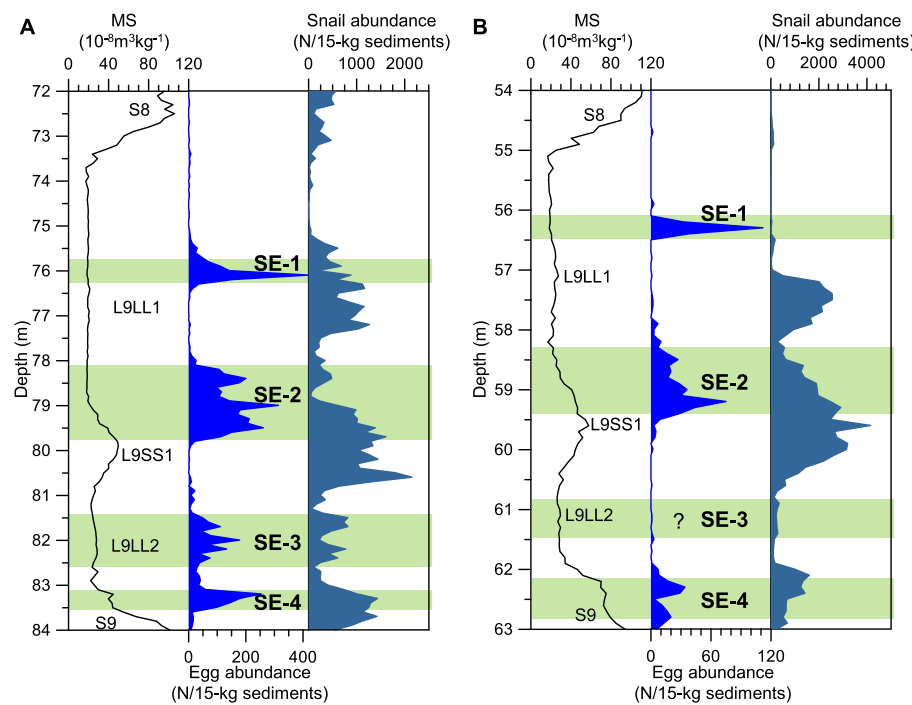


Fig. 5. The depth, magnetic susceptibility (MS), egg and snail abundances from the Xifeng (A) and Luochuan (B) sequences. Loess subunits (L9LL2 and L9LL1), paleosol units (S9 and S8) and subunit (L9SS1) are labeled following the stratigraphic nomenclature proposed by Kukla and An (1989). The abundances of eggs and snails are quantified as egg and snail counts in 15 kg of sediment, respectively. The green bars indicate high egg abundances documenting seasonal cooling events (SE-4 to SE-1).

Table 1

Seasonal cooling events (SE) from Chinese L9 loess strata. Depth, age, duration and intensity (maximum egg abundances) of the events observed in the Xifeng and Luochuan sequences, respectively.

Seasonal cooling event	Depth in Xifeng (m)	Age in Xifeng (ka)	Duration in Xifeng (kyr)	Intensity in Xifeng (maximum abundance) (N/15-kg sediments)	Depth in Luochuan (m)	Age in Luochuan (ka)	Duration in Luochuan (kyr)	Intensity in Luochuan (maximum abundance) (N/15-kg sediments)
SE-1	75.4–76.4	882–887	5	420	56.2–56.4	879–880	1	112
SE-2	78.2–79.8	895–910	15	314	58.2–59.4	897–911	14	75
SE-3	81.4–82.6	921–929	8	178	/	/	/	/
SE-4	83.1–83.5	935–941	6	253	62.2–62.9	936–945	9	34

characteristics of the four events are summarized in Table 1. They share the following three characteristics, as observed from Figs. 5 and 6 and Table 1. First, seasonal cooling events seem to occur during climate cooling transitions (green bars in Fig. 6) and near cooling extremes (glacial maxima) (yellow bars in Fig. 6). The former, labeled SE-4 and SE-2, occurs during climate cooling transitions from MIS 25 to MIS 24 and from MIS 23 to MIS 22, respectively, corresponding to a decreasing trend in MS values. The latter, labeled SE-3 and SE-1, seems to occur near glacial maxima, identified by the very low MS values and their stratigraphic location (Fig. 6A–D). If we use the maximum abundance or duration as an indication of the strength of seasonal events, SE-4 is stronger than SE-3 as indicated by its higher maximum abundance; SE-2 is stronger, as documented by its significantly longer duration, although a bit lower maximum abundance, than SE-1 (Table 1; Figs. 5 and 6). During the transition from loess to paleosol, corresponding to a deglacial trend, seasonal cooling events are not documented. Second, the intensity of seasonal cooling events becomes stronger after about 910 ka, i.e., the two younger events SE-2 and SE-1 are stronger than the two older ones SE-4 and SE-3. Third, changes in egg abundance are not synchronous with snail abundance, i.e., high egg abundance mostly corresponds to reduction in snail abundance (Fig. 5).

4. Discussion

The dominant land snail species in loess deposits of the CLP are minute species with adult shells measuring ~2–3 mm (Wu et al., 2002, 2007, 2018; Rousseau et al., 2009; Dong et al., 2021, 2022). In the L9 loess unit, the most abundant species are *Vallonia tenera* and *Pupilla aeoli* and the second abundant are *Pupilla cupa* and *Gastrocopta armigerella* (Wu and Wu, 2011). The largest dimension of the fossil eggs is 0.6–0.8 mm (Fig. 4). Eggs of this size range are produced by ~2–3-mm land snails (Barker, 2001; Welter-Schultes, 2012), which is consistent with the dominance of minute snail species in the loess-paleosol sequence across the CLP (Wu et al., 2002, 2007, 2018; Rousseau et al., 2009; Wu and Wu, 2011; Zhang Y.T. et al., 2020; Dong et al., 2021, 2022). However, we cannot determine whether these fossil eggs were produced by a single or multiple species, due to the absence of egg diagnostic characteristics for species-level identification.

Land-snails' egg-laying sites are undoubtedly influenced by numerous local environmental factors, such as local humidity conditions. However, these local environmental factors appear to have played a minor role in our results for two key reasons. First, similar trends were observed at sites approximately 160 km apart (Fig. 2) (Kukla and An, 1989), which are expected to have distinct microhabitats. Second, while local environmental factors likely influence egg development at the

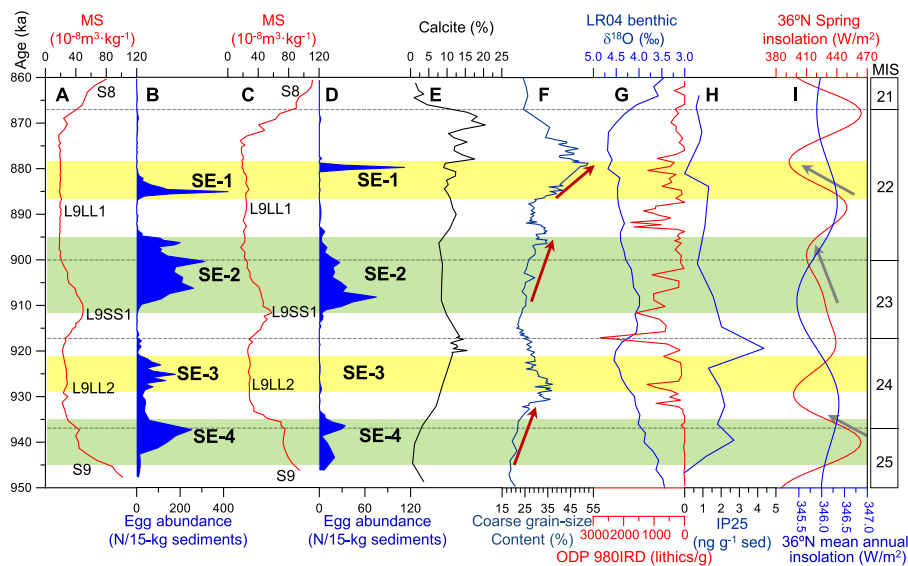


Fig. 6. Seasonal cooling events (SE-4 to SE-1) documented in the Chinese Loess Plateau by egg-abundance variations and their comparison with other climate records during Marine Isotope Stages (MIS) 24–22. A and B. Magnetic susceptibility (MS) and egg abundance from the Xifeng sequence, respectively, with loess subunits (L9LL2 and L9LL1), paleosol units (S9 and S8) and subunit (L9SS1) labeled in the MS record using the stratigraphic nomenclature proposed by Kukla and An (1989). C and D. MS record and egg abundance from the Luochuan sequence, respectively. E. Calcite content in the Luochuan section (Meng et al., 2018). F. The content in coarse grain size ($>30\text{ }\mu\text{m}$) from the Xifeng sequence (Lu et al., 1999, 2004, 2022). The red arrows indicate increases in coarse grain-size content. G. Stacked LR04 benthic $\delta^{18}\text{O}$ record (blue) (Lisicki and Raymo, 2005), and ice-raftered debris (IRD) record (red) from the Ocean Drilling Program (ODP) Site 980 ($55^{\circ}29'\text{N}$, $14^{\circ}42'\text{W}$) at high northern latitudes (red) (Wright and Flower, 2002). H. Sea ice reconstruction based on the Arctic sea ice biomarker IP25 from the International Ocean Discovery Program (IODP) Site U1343 ($57^{\circ}33'\text{N}$, $175^{\circ}49'\text{W}$) in the North Pacific (Detlef et al., 2018). I. 36°N spring (red) and mean annual (blue) insolation (Laskar et al., 2004). The grey arrows indicate decreases in spring insolation near Xifeng and Luochuan latitudes. Marine Isotope Stages (MIS) are labeled on the right. The horizontal green bars indicate seasonal cooling events during climate cooling shift, while the yellow bars indicate seasonal cooling events near glacial maximum. The horizontal dashed lines indicate MIS boundaries according to Lisicki and Raymo (2005)

timescale of the snail's lifespan (e.g., Barker, 2001), their impact appears negligible at longer timescales such as the decadal and orbital timescales (e.g., Li et al., 2021, 2022, 2023); thus, they are not the main factors accounting for our observed orbital-scale changes. Seasonal cooling events during the reproductive season and carbonate dissolution are potentially the main factors impacting changes in land-snail egg abundance. Before checking if the variations in the egg-abundance relate to any climate factor, we need first to compare it with some local factors like calcite content and MS of the sediment.

4.1. Carbonate content

Carbonate content in the Luochuan L9 unit mostly concentrates on the range of 11.6–20.5 % (Fig. 6E) (Meng et al., 2018), significantly higher than carbonate-dissolution threshold of 5 % in Chinese loess deposits (Liu, 1985; Wen, 1989) and in European loess (personal communication with Dr. Oliver Moine). Considering the generally increasing trend of carbonate content from the southeastern to northwestern CLP (Liu, 1985; Meng et al., 2018), the carbonate content at Xifeng should be higher than that at Luochuan. Moreover, changes in the egg abundance do not parallel with changes in the calcite content (Fig. 6B–D, E). Therefore, both Xifeng and Luochuan have carbonate contents that favor the preservation of land-snail eggs. Furthermore, over the CLP, loess layers including L9 have no or very weak soil development, as seen from MS measurements (Liu, 1985; Rousseau and Wu, 1997, 1999; Wu et al., 2007; Rousseau et al., 2009; Wu and Wu, 2011; Hao et al., 2012). MS values in the L9 loess layers are between 64 and $17 \times 10^{-8}\text{ m}^3\text{kg}^{-1}$, with an average of $26 \times 10^{-8}\text{ m}^3\text{kg}^{-1}$ in Xifeng, while in Luochuan the values are between 90 and $17 \times 10^{-8}\text{ m}^3\text{kg}^{-1}$, with an average of $35 \times 10^{-8}\text{ m}^3\text{kg}^{-1}$ (Figs. 5 and 6). These values are much lower than those in strongly developed paleosols in the CLP (e.g., Wu et al., 2007; Rousseau et al., 2009; Hao et al., 2012). Finally, nearly all of the eggs are intact, do not show any particular sign of diagenesis

(Fig. 4), and variations in egg abundance are mostly correlated inversely to changes in snail abundance (Fig. 5). Since both eggs and shells are primarily composed of carbonate, the scenario in paleosols where land snails are abundantly preserved while eggs undergo widespread dissolution is unlikely. Within the S9 and L9SS1 paleosols, indicative of warmer climate conditions, land-snail shells are relatively abundant while eggs are scarce (Fig. 5). This pattern excludes the possibility that the smaller number or lack of eggs is caused by the lack of land snails, but it aligns with the expected result: eggs hatch into snails, and the resulting shells are abundant.

In summary, the features of our observations exclude carbonate dissolution as the main factor impacting changes in egg abundance in the L9 loess units of the Xifeng and Luochuan sequences.

4.2. Impact of seasonal cooling events

Hatching or not would also induce changes in egg abundance. During the reproductive season in spring, cooling events induce rapid temperature decreases which are unfavorable for egg hatching since temperature is the most crucial limiting factor for egg hatching in the environment (Sun, 2001; Brown et al., 2004; Welter-Schultes, 2012). Therefore, egg abundance should be high when seasonal cooling events are strong, preventing any hatching activity. This has been documented by land-snail egg abundances from surface-soil deposits (Li et al., 2021) and loess-paleosol sequences of the last five glacial-interglacial cycles (Li et al., 2022, 2023). Moreover, more eggs were found in the Xifeng sequence than in the Luochuan sequence (Figs. 5 and 6; Table 1). Such observation is consistent with the present higher frequency and strength of cold spells noticed in Xifeng than in Luochuan, the former being located in the main pathway of cold spells (Qian, 1991; Li et al., 2021). Therefore, changes in land-snail eggs in the L9 loess layer would have mainly been impacted by seasonal cooling events. However, it should be emphasized that temperatures severely below the minimum hatching

threshold for a long period would be highly detrimental to snail development, causing both eggs and snails to disappear. In such cases, seasonal cooling events would be undetectable in the egg record.

The snail assemblages in loess units of the CLP are dominated by the cold-aridiphilous ecotype and the dominant species in this ecotype are the species with a shell size of ~2–3 mm (Wu et al., 2002, 2007, 2018; Rousseau et al., 2009; Wu and Wu, 2011; Dong et al., 2021, 2022). Although currently we have no information on hatching temperatures of these species, the hatching temperatures of such a size of snail species investigated are within the range of 10–25 °C (Li et al., 2021). During cold spells (a representative seasonal cooling event) in the CLP, the resulting temperature decreases of over 8–10 °C would have caused temperatures to be unsuitable for the egg hatching of most of the minute snails. Definitely, temperature requirement of specific species is urgently needed from future research.

4.3. Evolution of seasonal cooling events

Four seasonal cooling events (SE-4 to SE-1, from old to young) are documented in the CLP by high egg abundance (peak) during late MIS 25 and entire MIS 24–22, between 948 ka and 866 ka (Figs. 5 and 6; Table 1). From a more regional point of view, high egg abundance mainly corresponds to increases in coarse grain size and decreases in spring insolation in the CLP. More globally, these peaks in egg abundance also occur during the Northern Hemisphere ice sheet growth corresponding to stronger wind speed and harsher conditions at the source of the transported material, with a low concentration of ice-raftered debris (IRD) at high northern latitudes and contracted sea ice in the North Pacific. However, in details, these different events show particular characteristics that we have summarized as follows.

SE-4 occurs during the time interval from ~941 to 935 ka in Xifeng and ~945–936 ka in Luochuan (Table 1), which corresponds to the cooling transition from warm MIS 25 to cold MIS 24 (Fig. 6). The highest abundance reaches 253 eggs per 15-kg sediment in Xifeng. A slight increase from 19 % to 22 % in the content of coarse grain size is also documented in the Xifeng sequence, characterizing a strengthening of the East Asian winter monsoon (Fig. 6F) (Lu et al., 1999, 2004, 2022). SE-4 also corresponds to ice-sheet growth not exceeding the 4.5 % threshold of the benthic $\delta^{18}\text{O}$ record and to an absence of IRD from the Ocean Drilling Program (ODP) Site 980 (55°29'N, 14°42'W) at high northern latitudes (Fig. 6G) (Wright and Flower, 2002; Lisiecki and Raymo, 2005). Sea ice content in the North Pacific is moderate, as reconstructed from the sea ice biomarker IP25 from the International Ocean Discovery Program (IODP) Site U1343 (57°33'N, 175°49'W) (Fig. 6H) (Detlef et al., 2018). Local spring insolation significantly decreased from 464 to 430 W/m² when the Xifeng egg-abundance reaches maximum values, and egg abundances in the Xifeng and Luochuan sequences remain low during local spring, rather than mean annual, insolation maximum (Fig. 6I) (Laskar et al., 2004).

SE-3, which is only observed in the Xifeng sequence, is the weakest event of the studied interval, with the highest egg abundance reaching only 178 per 15-kg sediment, just prior to the glacial maximum of MIS 24 (Fig. 6B, G and Table 1). During this episode, the continental ice sheet volume is increasing, while the IRD concentration at high northern latitudes was low, indicating that the dynamics of the ice sheets did not yield strong iceberg calvings (Fig. 6G) (Wright and Flower, 2002; Lisiecki and Raymo, 2005). Sea ice cover was moderate (Fig. 6H), similar to that noticed during mid-late SE-4 (Detlef et al., 2018). Like SE-4, these particular conditions may favor the occurrence of seasonal cooling events over the CLP. However, an increase of about 38 W/m², from 397 to 435 W/m², in local spring insolation (Fig. 6I) (Laskar et al., 2004) is likely to have suppressed the enhancement of seasonal cooling events. This is consistent with a weakening of the East Asian winter monsoon, as documented by a decreasing content in coarse grain size in the CLP (Fig. 6F) (Lu et al., 1999, 2004, 2022). In summary, the environmental conditions during this second episode may have favored a

low intensity of seasonal cooling events in the CLP, resulting in the lowest egg abundance in Xifeng and an absence in Luochuan. The difference of seasonal cooling events in Xifeng and Luochuan is consistent with the modern observation that Xifeng is a geographical center of cold spells in the CLP (Qian, 1991).

SE-2 occurs in both sections during the transition from MIS 23 to MIS 22, corresponding to a climate cooling trend in a similar condition to SE-4. This event is the longest in duration, almost identical in both sequences, and the second highest in magnitude (Table 1). Coincident with this event, an increasing trend in coarse grain size, an increasing volume of Northern Hemisphere ice sheets with a decreasing trend in IRD concentration, and a substantial reduction in sea ice can be noticed (Fig. 6F and G) (Lu et al., 1999, 2004, 2022; Wright and Flower, 2002; Lisiecki and Raymo, 2005). During this third event, local spring insolation at 36°N reduced by 20 W/m² (from 430 to 410 W/m²) for a long time, which could have contributed to the long duration of SE-2 (Fig. 6I) (Laskar et al., 2004). All these lines of evidence characterize cooling climate conditions which may have been favorable for the occurrence and enhancement of seasonal cooling events.

As indicated in Fig. 6 and Table 1, SE-1 differs from the other three events as it is composed of two very high but narrow peaks in egg abundance. Like SE-3, it also occurs near the glacial maximum. During this time interval, coarse grain size increases greatly in the CLP, from 29 % to 52 %, reaching the maxima in the entire L9 unit (Lu et al., 1999, 2004, 2022). The stack benthic $\delta^{18}\text{O}$ values surpassing 4.5 % (Lisiecki and Raymo, 2005) in the upper part of this episode indicate maximum Northern Hemisphere ice sheet volume. The IRD concentration shows moderate values, nevertheless higher than those observed during the other three events noticed previously (Wright and Flower, 2002). These parameters indicate a significant expansion of the Northern Hemisphere ice sheets during this period, with a reduced sea ice cover and a moderate IRD concentration slightly higher than those from the other three events (Detlef et al., 2018). Spring insolation decreases in the largest amount (i.e., more than 50 W/m²) from 447 to 393 W/m² (Laskar et al., 2004), which could be the key factor leading to the strength and narrowness of SE-1.

SE-2 and SE-1, described from L9LL1, are stronger than SE-3 and SE-4 identified in L9LL2 and upper S9, as expressed by the egg abundance. The two groups correspond to two different status of sea ice cover with a major reduction in sea ice at about 910 ka (Fig. 6H). Before 910 ka, SE-4, which occurs during a climate cooling trend, is stronger than SE-3 that occurs near glacial maximum. A similar characteristic and pattern are also observed after 910 ka, i.e., the cooling-transition event SE-2 has a much longer duration than the glacial-maximum event SE-1 that occurs just prior to MIS 22 cooling maximum (Table 1). Such differences in the climate conditions prior to and after 910 ka support the abrupt increase in the $\delta^{18}\text{O}$ of the glacial stages following 900 ka after MIS 23, as depicted by Hodell and Channell (2016) when comparing data from ODP Sites 1123 and 806.

This study also shows that during the late MPT, seasonal cooling events are strong during the climate cooling transitions of MIS 25 to MIS 24 and MIS 23 to MIS 22, but not during the warming intervals, such as the deglacials (from L9LL2 to L9SS1 and from L9LL1 to S8) and the peak of L9SS1 (corresponding to the interglacial maximum of MIS 23). Such a pattern is similar to our previous observations from the last five climate cycles which showed that strong seasonal cooling events mainly occur during climate cooling shifts, including glacial inceptions and the shifts of MIS 7e to MIS 7d, MIS 5e to MIS 5d, MIS 5c to MIS 5b and MIS 3 to MIS 2 (Li et al., 2022, 2023).

However, differences in the occurrence of seasonal cooling events were also observed during the studied time intervals and the last five climate cycles. First, during the MIS 11 interglacial, two weaker seasonal cooling events were observed (Li et al., 2023). However, they are not observed during all other interglacials of the studied time interval and the last five glacial-interglacial cycles (Li et al., 2022, 2023). This may indicate that seasonal cooling events could have evolved differently

during the low-eccentricity MIS 11 interglacial (Li et al., 2023). Second, during the studied ending interval of the MPT, seasonal cooling events not only occurred during climate cooling transitions, but also occurred just prior to the glacial maxima of MIS 24 and MIS 22. However, during the last five glacial-interglacial cycles, seasonal cooling events mainly occurred during climate cooling transitions, rather than during glacial maxima apart from the last glacial maximum (LGM) during which a stronger seasonal cooling event is documented by a relatively high egg abundance (Li et al., 2022). The occurrence of seasonal cooling event during the LGM corresponds to the unusual transition from the mild MIS 3 interglacial to the severe glacial maximum of MIS 2, which was marked by strong expansion of ice volumes in high northern latitudes. Therefore, could such a difference in the occurrence of seasonal cooling events between the end of MPT and the last 490 ka be related to different climate conditions represented by different continental ice-volume estimates?

The stack benthic $\delta^{18}\text{O}$ values vary between 4.5 ‰ and 3.5 ‰, indicating the occurrence of Northern Hemisphere ice sheets which would have induced strong Siberian High reinforcing the East Asian winter monsoon and possibly increased seasonal cooling events over the CLP during glacial inceptions (Qian, 1991; Lisiecki and Raymo, 2005; Hao et al., 2012). During cold spells, rapid temperature decreases of over 8–10 °C (Qian, 1991) would have exceeded the lowest limiting temperature requirement for egg hatching, leading to substantial hatching failures (Li et al., 2021). However, it is possible that sufficiently large ice sheets might be associated with climate regimes of diminished variability (McManus et al., 1999). Therefore, climatic events would be weak or absent when the Northern Hemisphere ice sheets were sufficiently large, as expressed by the benthic $\delta^{18}\text{O}$ values greater than the 4.5 ‰ threshold (McManus et al., 1999). Under such conditions, the margins of the Northern Hemisphere ice sheets could reach the subpolar North Atlantic (Wright and Flower, 2002), resulting in low variable climate conditions at high northern latitudes which did not favor the occurrence of seasonal cooling events over the CLP.

Seasonal cooling events occur during glacial maxima prior to 800 ka when glacial-interglacial cycles have a dominated 41-kyr periodicity, but they do not occur during glacial maxima of the last several glacial-interglacial cycles dominated by a 100-kyr periodicity. This may be related to different volumes of the ice sheets at high northern latitudes during the two intervals of different dominated periodicities (Fig. 1A) (Lisiecki and Raymo, 2005). Numerous studies indicate that ice sheet expands significantly after 900–800 ka associated with the occurrence onward of the massive iceberg calvings named Heinrich events (e.g., Heinrich, 1988; Lisiecki and Raymo, 2005; Hodell and Channell, 2016; Rousseau et al., 2022). Therefore, the Northern Hemisphere ice volumes during the last several glacial maxima, apart from the LGM, could have been sufficiently large to exceed a threshold and induce harsher climate conditions (McManus et al., 1999) that do not favor the occurrences of seasonal cooling events and egg abundance. Therefore, analysis of egg abundance variations during the MPT provides critical evidence that Northern Hemisphere ice volume constituted the primary driver modulating the evolution of seasonal cooling events across distinct climatic intervals.

Low sea ice cover over Siberian marginal seas presently strengthens the winter Siberian High (Wu et al., 2011). Moreover, reduction in this sea ice cover also strengthens ocean-atmosphere exchange of heat and moisture and decreases albedo (Wu et al., 2011). All these changes favor strong air movement at high northern latitude and cause strong cold spells in the CLP, mainly via atmospheric transport by the East Asian winter monsoon (e.g., Wu et al., 2011; Hao et al., 2012). This is therefore the modern mechanism of sea ice on climate change that we propose to explain the observed egg-abundance variations in the L9 loess unit.

A decreasing trend of local spring insolation is likely to have also favored the occurrence of seasonal cooling events through its impact on temperature (Fig. 6). Lower spring insolation at the studied sites would have stronger contributions to temperature decreases that can facilitate

the temperatures beyond the lower threshold and lead to considerable hatching failures (Qian, 1991; Laskar et al., 2004; Li et al., 2021). On the contrary, spring-insolation maxima favor increases in temperature and likely provide suitable climate conditions for land-snail eggs to hatch, corresponding mostly to the time intervals when seasonal cooling events did not occur (Fig. 6). Therefore, strong events (SE-4 and SE-2) correspond to a decreasing trend in spring insolation, weak events (SE-3) are coincident with an increasing trend in spring insolation, and no (strong) events occur during spring insolation peaks, including the middle part of SE-4 (Fig. 6).

5. Conclusion

Land-snail egg records from the upper S9 and entire L9 units in the CLP indicate long-term evolution of seasonal cooling events during late MIS 25 and entire MIS 24–22. Four seasonal cooling events, SE-1, SE-2, SE-3 and SE-4, are documented by egg-abundance peaks. They tend not to occur during warm intervals such as deglacials and interglacial maximum, but occur during climate cooling transitions of MIS 25/24 and MIS 23/22 and just prior to the glacial maxima of MIS 24 and MIS 22. The events near glacial maxima are weaker than those during climate cooling transitions. Seasonal cooling events occur during glacial maxima during the studied interval, but they do not occur during glacial maxima of the last several glacial-interglacial cycles, apart from the LGM. Moreover, the last two events SE-1 and SE-2 appear to be stronger than the earlier two events SE-3 and SE-4, which indicates that the intensities of seasonal cooling events enhanced around 910 ka. The four events correspond well to ice-sheet growth with low IRD concentrations and sea-ice reductions at high northern latitudes, which would have caused strong cooling events over the CLP during the reproductive season and therefore unfavorable temperatures for the hatching of land-snail eggs. The difference in seasonal cooling events during the MPT and the last several climatic cycles could be related to different volumes of the ice sheets at high northern latitudes. Moreover, local spring insolation may also contribute to the intensities of seasonal cooling events, as seen from strong events (SE-4 and SE-2) corresponding to a decreasing trend in spring insolation, weak events (SE-3) coincident with an increasing trend in spring insolation, and no events occurring during most insolation peaks. Our study provides new evidence for the evolution of seasonal cooling events during a key time interval of the MPT.

Author contributions

NW and FL conceived and designed the study. FL, LH, BW, XC and NW performed the sampling. FL and LH performed the collecting and counting of eggs. LH and BW performed the collecting and counting of snails and the measurements of magnetic susceptibility. QH and FL established the chronology of the studied sections. FL, NW and DDR wrote the manuscript. FL, NW, DDR, LH, YD and QH contributed to the interpretation of the results.

Declaration of competing interest

All the authors declare that they have no conflict of interest.

Acknowledgments

We thank Prof. Jianping Zhang for assistance in the fieldwork. We are grateful to the two reviewers for their insightful comments and constructive suggestions that improved the manuscript greatly. This study was supported by the National Natural Science Foundation of China (grants 42172210, 42488201 and 42272216). This is a Lamont-Doherty Earth Observatory (LDEO) contribution.

Appendix A. Supplementary data

Supplementary data to this article can be found online at <https://doi.org/10.1016/j.quascirev.2025.109584>.

Data availability

All data and/or code is contained within the submission.

References

- Barker, G.M., 2001. The Biology of Terrestrial Molluscs. CABI Publishing, Hamilton, p. 558.
- Brown, J.H., Gillooly, J.F., Allen, A.P., Savage, V.M., West, G.B., 2004. Toward a metabolic theory of ecology. *Ecology* 85, 1771–1789.
- Clark, P.U., Archer, D., Pollard, D., Blum, J.D., Rial, J.A., Brovkin, V., Mix, A.C., Pisias, N.G., Roy, M., 2006. The middle Pleistocene transition: characteristics, mechanisms, and implications for long-term changes in atmospheric pCO₂. *Quat. Sci. Rev.* 25, 3150–3184.
- Crowley, T.J., Short, D.A., Mengel, J.G., North, G.R., 1986. Role of seasonality in the evolution of climate during the last 100 million years. *Science* 231, 579–584.
- Denton, G.H., Alley, R.B., Comer, G.C., Broecker, W.S., 2005. The role of seasonality in abrupt climate change. *Quat. Sci. Rev.* 24, 1159–1182.
- Detleff, H., Belt, S.T., Sosdian, S.M., Smik, L., Lear, C.H., Hall, I.R., Cabedo-Sanz, P., Husum, K., Kender, S., 2018. Sea ice dynamics across the mid-pleistocene transition in the Bering Sea. *Nat. Commun.* 9, 941. <https://doi.org/10.1038/s41467-018-02845-5>.
- Ding, Z., Liu, T., Yu, Z., Guo, Z., Zhu, R., 1995. Ice-volume forcing of East Asian winter monsoon variations in the past 800,000 years. *Quat. Res.* 44, 149–159.
- Ding, Z.L., Derbyshire, E., Yang, S.L., Yu, Z.W., Xiong, S.F., Liu, T.S., 2002. Stacked 2.6-Ma grain size record from the Chinese loess based on five sections and correlation with the deep-sea δ¹⁸O record. *Paleoceanography* 17, 1033. <https://doi.org/10.1029/2001PA000725>.
- Dong, Y.J., Wu, N.Q., Li, F.J., Zhang, D., Zhang, Y.T., Huang, L.P., Chen, X.Y., Wu, B., Lu, H.Y., 2020. Anthropogenic modification of soil communities in northern China for at least two millennia: evidence from a quantitative mollusk approach. *Quat. Sci. Rev.* 248, 106579.
- Dong, Y.J., Wu, N.Q., Li, F.J., Huang, L.P., Lu, H.Y., Stenseth, N.C., 2021. Paleorecords reveal the increased temporal instability of species diversity under biodiversity loss. *Quat. Sci. Rev.* 269, 107147.
- Dong, Y.J., Wu, N.Q., Li, F.J., Zhang, D., Zhang, Y.T., Shen, C.M., Lu, H.Y., 2022. The Holocene temperature conundrum answered by mollusk records from east Asia. *Nat. Commun.* 13, 5153. <https://doi.org/10.1038/s41467-022-32506-7>.
- Guo, Z.T., Liu, T.S., Fedoroff, N., Wei, L.Y., Ding, Z.L., Wu, N.Q., Lu, H.Y., Jiang, W.Y., An, Z.S., 1998. Climate extremes in loess of China coupled with the strength of deep-water formation in the north Atlantic. *Global Planet. Change* 18, 113–128.
- Han, H.H., Wang, Y.R., Huang, F., Wang, P., 2013. The characteristics of low temperature in spring over loess Plateau. *J. Gansu Sci.* 25, 58–61.
- Hao, Q.Z., Wang, L., Oldfield, F., Peng, S.Z., Qin, L., Song, Y., Xu, B., Qiao, Y.S., Bloemendal, J., Guo, Z.T., 2012. Delayed build-up of arctic ice sheets during 400000-year minima in insolation variability. *Nature* 490, 393–396.
- Haug, G.H., Ganopolski, A., Sigman, D.M., Rosell-Mele, A., Swann, G.E.A., Tiedemann, R., Jaccard, S.L., Bollmann, J., Maslin, M.A., Leng, M.J., Eglinton, G., 2005. North Pacific seasonality and the glaciation of North America 2.7 million years ago. *Nature* 433, 821–825.
- Heinrich, H., 1988. Origin and consequences of cyclic ice rafting in the northeast Atlantic Ocean during the past 130,000 years. *Quat. Res.* 29, 142–152.
- Heller, F., Liu, T.S., 1982. Magnetostratigraphical dating of loess deposits in China. *Nature* 300, 431–433.
- Hodell, D.A., Channell, J.E.T., 2016. Mode transitions in northern hemisphere glaciation: co-evolution of millennial and orbital variability in Quaternary climate. *Clim. Past* 12, 1805–1828.
- Jin, C.S., Liu, Q.S., 2011. Remagnetization mechanism and a new age model for L9 in Chinese loess. *Phys. Earth Planet. Inter.* 187, 261–275.
- Kukla, G., 1987. Loess stratigraphy in central China. *Quat. Sci. Rev.* 6, 191–219.
- Kukla, G., An, Z.S., 1989. Loess stratigraphy in central China. *Palaeogeogr. Palaeoclimatol. Palaeoecol.* 72, 203–225.
- Kukla, G., An, Z.S., Melice, J.L., Gavin, J., Xiao, J.L., 1990. Magnetic susceptibility record of Chinese loess. *Trans. R. Soc. Edinb. Earth Sci.* 81, 263–288.
- Laskar, J., Robutel, P., Joutel, F., Gastineau, M., Correia, A.C.M., Levrard, B., 2004. A long-term numerical solution for the insolation quantities of the Earth. *Astron. Astrophys.* 428, 261–285.
- Li, F.J., Yang, Y.Q., Wu, N.Q., Huang, L.P., Dong, Y.J., 2019. Fossil snail eggs discovered from the Chinese loess Plateau and their indications of seasonal abrupt climate event. *Quat. Sci.* 39, 1068–1070.
- Li, F.J., Wu, N.Q., Dong, Y.J., Zhang, D., Zhang, Y.T., Yang, Y.Q., Huang, L.P., Xu, D.K., Zhang, J.P., Lu, H.Y., 2021. Land-snail eggs as a proxy of abrupt climatic cooling events during the reproductive season. *Sci. Bull.* 66, 1274–1277.
- Li, F.J., Wu, N.Q., Zhang, D., Rousseau, D.D., Yang, Y.Q., Hao, Q.Z., Dong, Y.J., Lu, H.Y., 2022. Glacial-interglacial evolution of seasonal cooling events documented by land-snail eggs from Chinese loess. *Quat. Sci. Rev.* 284, 107506.
- Li, F.J., Wu, N.Q., Dong, Y.J., Yang, Y.Q., Zhang, Y.T., Zhang, D., Hao, Q.Z., Lu, H.Y., 2023. Seasonal climatic instability in the western Chinese loess Plateau during marine isotope stages 12–10. *Sci. Rep.* 13, 5725. <https://doi.org/10.1038/s41598-023-32923-8>.
- Lisiecki, L.E., Raymo, M.E., 2005. A Pliocene-Pleistocene stack of 57 globally distributed benthic δ¹⁸O records. *Paleoceanography* 20, PA1003. <https://doi.org/10.1029/2004PA001071>.
- Liu, T., 1964. Loess Deposits in the Middle Reaches of the Yellow River. Science Press, Beijing, p. 234.
- Liu, T., 1985. Loess and the Environment. China Ocean Press, Beijing, p. 251.
- Liu, T.S., Wang, T.M., Wang, K.L., Wen, C.C., 1958. Chinese loess map of Shansi and Shensi regions. *Sci. Rec.* 2, 167–174.
- Lu, H.Y., Huissteden, K.V., An, Z.S., Nugteren, G., Vandenberghe, J., 1999. East Asia winter monsoon variations on a millennial time-scale before the last glacial-interglacial cycle. *J. Quat. Sci.* 14, 101–110.
- Lu, H.Y., van Huissteden, K., Zhou, J., Vandenberghe, J., Liu, X.D., An, Z.S., 2000. Variability of East Asian winter monsoon in Quaternary climatic extremes in north China. *Quat. Res.* 54, 321–327.
- Lu, H.Y., Zhang, F.Q., Liu, X.D., Duce, R.A., 2004. Periodicities of palaeoclimatic variations recorded by loess-paleosol sequences in China. *Quat. Sci. Rev.* 23, 1891–1900.
- Lu, H.Y., Wang, X.Y., Wang, Y., Zhang, X.J., Yi, S.W., Wang, X.Y., Stevens, T., Kurbanov, R., Markovic, S.B., 2022. Chinese loess and the Asian monsoon: what we know and what remains unknown. *Quat. Int.* 620, 85–97.
- Lu, Y.C., An, Z.S., 1979. Discussion on paleoenvironmental changes in the loess Plateau since about 700 ka. *Chin. Sci. Bull.* 24, 221–224.
- McManus, J.F., Oppo, D.W., Cullen, J.L., 1999. A 0.5-million-year record of millennial-scale climate variability in the north Atlantic. *Science* 283, 971–975.
- Meng, X.Q., Liu, L.W., Wang, X.T., Balsam, W., Chen, J., Ji, J.F., 2018. Mineralogical evidence of reduced East Asian summer monsoon rainfall on the Chinese Loess plateau during the early Pleistocene interglacials. *Earth Planet Sci. Lett.* 486, 61–69.
- Moine, O., Rousseau, D.D., Antoine, P., 2008. The impact of Dansgaard-Oeschger cycles on the loess environment and malacofauna of Nussloch (Germany) during the upper Weichselian. *Quat. Res.* 70, 91–104.
- Porter, S.C., An, Z.S., 1995. Correlation between climate events in the north Atlantic and China during last glaciation. *Nature* 375, 305–308.
- Puisségur, J.J., 1976. Mollusques continentaux quaternaires de Bourgogne. Significations stratigraphiques et climatiques. Rapports avec d'autres faunes boréales de France: Université de Dijon Mémoires Géologiques 3, 241.
- Qian, L.Q., 1991. Climate of Loess Plateau. Meteorological Press, Beijing, p. 369.
- Rousseau, D.D., Wu, N.Q., 1997. A new molluscan record of the monsoon variability over the past 130 000 yr in the Luochuan loess sequence, China. *Geology* 25, 275–278.
- Rousseau, D.D., Wu, N.Q., 1999. Mollusc record of monsoon variability during the L2-S2 cycle in the Luochuan loess sequence, China. *Quat. Res.* 52, 286–292.
- Rousseau, D.D., Wu, N.Q., Pei, Y.P., Li, F.J., 2009. Three exceptionally strong East-Asian summer monsoon events during glacial times in the past 470 kyr. *Clim. Past* 5, 157–169.
- Rousseau, D.D., Bagniewski, W., Ghil, M., 2022. Abrupt climate changes and the astronomical theory: are they related? *Clim. Past* 18, 249–271.
- Sümegi, P., Gulyás, S., Persaitis, G., GergelyPál, D., Molnár, D., 2011. The loess-paleosol sequence of Basahar (Hungary) revisited: Mollusc-based paleoecological results for the Middle and upper Pleistocene. *Quat. Int.* 240, 181–192.
- Sun, J.M., Liu, T.S., 2000. Stratigraphic evidence for the uplift of the Tibetan Plateau between 1.1 and 0.9 Myr ago. *Quat. Res.* 54, 309–320.
- Sun, R.Y., 2001. Principles of Animal Ecology. Beijing Normal University Press, Beijing, p. 636.
- Sun, Y.B., An, Z.S., Clemens, S.C., Bloemendal, J., Vandenberghe, J., 2010. Seven million years of wind and precipitation variability on the Chinese Loess Plateau. *Earth Planet Sci. Lett.* 297, 525–535.
- Wang, K.L., Wen, C.C., Guan, E.W., Zhang, H.Y., Ding, M.L., Song, M.H., Zhang, Y., Yang, G.L., 1962. Investigative report on the Quaternary geology in the reaches of the Jing and Luo Rivers in northern Shaanxi and eastern Gansu, in Investigative Group of Water and Soil Conservation in the middle reaches of the Yellow River Chinese Academy of Sciences, Institute of Geology Chinese Academy of Sciences. In: Investigative Report of Quaternary Geology in the Middle Reaches of the Yellow River. Science Press, Beijing, pp. 99–168.
- Wang, D.J., Wang, Y.C., Han, J.T., Duan, M.G., Shan, J.Z., Liu, T.S., 2010. Geomagnetic anomalies recorded in L9 of the Songjiadian loess section in southeastern Chinese Loess Plateau. *Chin. Sci. Bull.* 55, 520–529.
- Wang, X.S., Lövlie, R., Yang, Z.Y., Pei, J.L., Zhao, Z.Z., Sun, Z.M., 2005. Remagnetization of Quaternary eolian deposits: a case study from SE Chinese Loess Plateau. *Geochem. Geophys. Geosyst.* 6, Q06H18. <https://doi.org/10.1029/2004GC000901>.
- Welter-Schultes, F., 2012. European Non-marine Molluscs, a Guide for Species Identification. Planer Poster Editions, Gottingen, p. 679.
- Wen, Q.Z., 1989. Geochemistry of Loess in China. Science Press, Beijing, p. 285.
- Wright, A.K., Flower, B.P., 2002. Surface and deep ocean circulation in the subpolar North Atlantic during the mid-pleistocene revolution. *Paleoceanography* 17, 1068. <https://doi.org/10.1029/2002PA000782>.
- Wu, B.Y., Su, J.Z., Zhang, R.H., 2011. Effects of autumn-winter Arctic sea ice on winter Siberian High. *Chin. Sci. Bull.* 56, 3220–3228.
- Wu, B., Wu, N.Q., 2011. Terrestrial mollusc records from Xifeng and Luochuan L9 loess strata and their implications for paleoclimatic evolution in the Chinese Loess Plateau during marine Oxygen Isotope Stages 24–22. *Clim. Past* 7, 349–359.
- Wu, N.Q., Liu, T.S., Liu, X.P., Gu, Z.Y., 2002. Mollusc record of millennial climate variability in the Loess Plateau during the last Glacial Maximum. *Boreas* 31, 20–27.
- Wu, N.Q., Chen, X.Y., Rousseau, D.D., Li, F.J., Pei, Y.P., Wu, B., 2007. Climatic conditions recorded by terrestrial mollusc assemblages in the Chinese Loess Plateau during marine Oxygen Isotope stages 12–10. *Quat. Sci. Rev.* 26, 1884–1896.

- Wu, N.Q., Li, F.J., Rousseau, D.D., 2018. Terrestrial mollusk records from Chinese loess sequences and changes in the East Asian monsoonal environment. *J. Asian Earth Sci.* 155, 35–48.
- Zhang, J.P., Lu, H.Y., Jia, J.W., Shen, C.M., Wang, S.Y., Chu, G.Q., Wang, L., Cui, A.N., Liu, J.Q., Wu, N.Q., Li, F.J., 2020. Seasonal drought events in tropical East Asia over the last 60,000 y. *Proc. Natl. Acad. Sci. U. S. A.* 117, 30988–30992.
- Zhang, Y.T., Wu, N.Q., Li, F.J., Hao, Q.Z., Dong, Y.J., Zhang, D., Lu, H.Y., 2020. Eco-environmental changes in the Chinese Loess Plateau during low-eccentricity interglacial Marine Isotope Stage 19. *Sci. China Earth Sci.* 63, 1408–1421.
- Zhou, L.P., Shackleton, N.J., 1999. Misleading positions of geomagnetic reversal boundaries in Eurasian loess and implications for correlation between continental and marine sedimentary sequences. *Earth Planet Sci. Lett.* 168, 117–130.